MULTIFUNCTIONAL STRUCTURE CALIBRATION BY OPTIMAL MEASUREMENT USING HYBRID APPROACH FOR RESPONSE MONITORING

C.N. Sathyanarayana[*,#] and S. Raja[*]

Abstract

Multifunctional structure calibration by optimal measurement using hybrid approach is developed for the conventional strain gauges for response monitoring. In the hybrid calibration approach, we have used the finite element analysis and experimental modal technique to quantify the measured output of distributed sensors. Smart materials such as piezoelectric (PZT and PVDF) in thin film form are widely appreciated for distributed sensing application in composite structures. The light weight composite structures can be made multi-functional by incorporating the piezoelectric materials to have non-structural functionalities such as sensing, actuation, energy harvesting and health monitoring. In the present study, in addition to load carrying and damping, which are the essential structural functions, the composite plate is made to have self sensing capability with four distributed strain gauges and PZT patches respectively. Further, it has been shown that using a single strain measurement, the finite element strains can be updated at different assumed strain gauge locations in order to calibrate the PZT patch sensors placed nearby to output engineering strains.

***Keywords**: Multifunctional Structure, PZT, Strain Gauges, Sensor, Dynamic Calibration Factor and Composite Plate*

Introduction

Structural Health Monitoring (SHM) techniques have increasingly become popular in engineering and biological systems. Measurements, processing and fault diagnosis are the important elements in any SHM technique. In recent years, the response monitoring sensors are made as inherent elements of the structure itself to make the structure truly multifunctional. Sensing is a non-structural function but plays a key role in monitoring/predicting damages if any or helps to compute the fatigue life and aeroelastic stability/ or response. Thin PZT patches/films are well suited for the above purposes under a SHM scheme. However in order to get a quantifiable engineering data from a PZT patch, there is a need for in-situ calibration for the sensor, being on the structure. An attempt was made to calibrate the strain gauges under the frequency dependent dynamic loads to obtain the dynamic calibration factors for different modes [1]. These dynamic calibration factors can be used for the purpose of response monitoring and as well as calibrating the non-conventional PZT patches.

Wei and Pizhong [2] reviewed comprehensively modal parameter-based damage identification methods for beam and plate type structures and discussed the damage identification schemes in terms of signal processing algorithms. They classified the damage identification methods into four categories based on the vibration features: natural frequency-based methods, mode shape-based methods, curvature mode shapes methods and methods using both mode shapes and frequencies and further examined their merits and drawbacks. As an implementation, a comparative study was conducted using five extensively-used damage detection algorithms for beam-type structures to evaluate and demonstrate the validity and effectiveness of the signal processing algorithms.

Jinping and Hui [3] critically reviewed the development of advanced sensing technology and sensors in mainland China in the past decade, such as optic fiber sensing technology, wave propagation-based piezoelectric ceramic (PZT) sensing technology, smart cement-based sensing technology, and corrosion detection technology. They summarized the application of SHM technologies in earthquake engineering, wind engineering and discussed about life-cycle performance evaluation and corresponding progress achieved. The challenges and future trends in

* Scientist, Structural Technologies Division, National Aerospace Laboratories, Kodihalli, Post Box No. 1779, Bangalore-560 017, India, [#]Email : cns@nal.res.in, Ph.D Student, VTU, Belgaum, Karnataka

the development of sensing technology and SHM were also mentioned in the article.

Phillps et al. [4] presented a study on the performance of different vibration based damage identification (VBDI) techniques through numerical simulation and experiments using displacement and distributed strain measurements. They carried out experiments on a simply supported beam using accelerometers and long-gauge fiber bragg grating (FBG) sensors for different damages and found that distributed strain measurements from FBG sensors could successfully detect and localize single and multiple damages in the structures. They had established the importance of modal macro-strain vectors (MMSV) based damage index method for effective damage identification.

Adewuyi and Wu [5] developed a statistical vibration-based damage identification algorithm to assess the stability of the measurement data for detecting and locating the damage in civil structures, where variability in response and modal parameters due to measurement noise and environmental influence was often inevitable. They used the magnitudes of frequency response function (FRF) of the target sensors in a regression analysis and compared with the reference data for reliability assessment and damage localization. It was found that statistical approach is very effective for damage localization using strain data.

Kamrujjaman and Wu [6] proposed a damage identification technique based on the distributed Macro-Strain (MS) response measurements. It was assumed that ratio of the strain measured at a target location and a reference location of a beam-like structure was constant for a given dynamic condition of the structure. They also verified the proposed damage identification technique using the laboratory experiments and identified the damage in a noise-polluted environment. Long-gauge distributed sensors were deployed to collect the traffic induced strain measurement. Ajay Kesavan et al. [7] proposed a strain energy based SHM system for detecting the presence of multiple delemination on a 2D polymeric T-joint used in the marine structures. Both the damage locations and its intensity were monitored independent of external loadings. Takeda et al. [8] developed a small-diameter optical fiber and used it as FBG sensor for damage monitoring in composite structures.

Even though PZT patches, strain gauges, FBG sensors and accelerometers, velocity impedence head have been employed in various SHM schemes, the practical issue such as calibration is not yet properly addressed in order to obtain the multiple engineering states from a single sensor. Also, the quantity of any sensor data since directly depends on supports flexibility or host structure, where it is mounted, in-situ calibration becomes an important parameter in SHM technique. This also makes sense in monitoring the sensor faultiness while in use.

The current work addresses this important in-situ calibration for PZT patches along with a new procedure to limit the number of reference sensors, which will be used for multi-state sensing application [1]. Therefore a hybrid approach, involving FEA and vibration measurement has been proposed for calibrating the muti-functional structure by a limited number of measurements. The importance of damping on the dynamic calibration factor is also examined. The FE model of the composite plate is made in MSC-NASTRAN and subsequently a dynamic response analysis is carried out to compute the bending strains at different elements. The dynamic measurements are done and the strains are measured using the multi-channel dynamic data acquisition system (PROSIG) and processed further using DATS software. The element strain indeed represents the strain gauge output; however, it is noticed that there is a discrepancy in the computation. The error between the FE strain data and the measured strain is first computed at the reference sensing location. The error correction is then applied to all the elements and their strains are updated. For multifunctional structure calibration, these updated strains can be employed. In order to validate the developed procedure, the experimental plate structure is instrumented (also sub-structured), with four strain gauges and four PZT patches (Fig.2) distributed over them. For the plate structure, only one reference sensor is considered, in the substructure 2.

Substructured Based Response Monitoring

Figure 1 shows an elastic continuum, which has been sub-structured for the purpose of calibration. Each sub-structure is assumed to have a sensor to monitor its health locally. All the monitored local responses further can be integrated to predict the global response of the complete structure [9]. The plate structure, considered for response monitoring is divided into five sub-structures as shown in Fig.2. In each sub-structure (SS), one strain gauge and a PZT patch is surface bonded, except the fifth one which is assumed to have virtual sensors (FEM elements). The sub-structure SS2 is treated as reference, thus calibration for all the PZT patches is done with respect to the reference strain gauge that is placed nearby (strain gauge 1). How-

ever other strain gauges, namely S2, S3 and S4 are employed for validation purposes.

Fabrication of Specimen and Experimental Setup

The test specimens are made out of laminated composites using BID-Glass fabric with room temperature cure epoxy resin of size 400x400x1.5mm^3. The laminate is fabricated using 8mil BID-glass fabric with LY 556 epoxy resin having HY 951 hardener. Room Temperature Vacuum Bag Moulding (RTVBM) processing technique is used to fabricate the laminate. The composite laminate is subsequently cut into plates of 190mm long, 150mm wide with a diamond saw cutter. A 40mm length of the specimen is used for the purpose of clamping to simulate a cantilever plate boundary condition. Thus, the effective area of the test specimen is of 150x150x1.5mm^3. The mechanical properties of BID Glass with Epoxy Resin system are given in Table-1.

Four rosette type strain gauges are surface bonded on the top of the specimen for the purpose of kinematic strain measurement in normal (X and Y) and shear (XY) directions. Out of four gauges one strain gauge is treated as reference gauge (S_{ref}) and other gauges are considered as monitoring strain gauges (S_2, S_3 and S_4). The details of the strain gauges are tabulated in Table-2. Four PZT patches are also surface bonded to measure the responses from the structure to determine the dynamic calibration factor with respect to stain values.

Table-1 : Mechanical Properties of BID-Glass Fabric with Epoxy Resin System

Longitudinal Modulus (GPa)	24
Transverse Modulus (GPa)	21
Longitudinal Shear Modulus (GPa)	4.10
Transverse Shear Modulus (GPa)	4.10
Poisson's Ratio	0.2
Mass Density (Kg/m^3)	1720

Table-2 : Strain Gauge Details

Foil Strain Gauge	Rosette
Type	N32-FA-5-120-23
Gauge Length	5mm
Resistance	120.0 ± 0.3%Ω
Gauge Factor	2.11 ± 1%
Thermal Output	± 2με /° C
Lot No.	6105-911

The experimental set-up used for multi-sensor calibration experiments is shown in Fig.3. The clamped boundary condition, simulating a cantilever plate is found to be a very sensitive factor in the experiments; so the specimen is clamped to a table using two mild steel plates (40x150x20mm^3) on top and bottom with four M8 bolts. The bolts are tightened to 32 N-m using a torque wrench. A vibration generator, type SP2 sparanktronics, India make is used to excite the laminated plate along with the PCB force transducer (208C02), which has 11 mv/N sensitivity. An accelerometer of PCB make (353C02), having sensitivity of 100 mv/g is employed to measure the acceleration response. The input force signal and acceleration response signal are directly passed to the LMS SCADAS III hardware and signals are processed using LMS Test Lab software. In order to measure the critical strain response, strain gauge is connected to Prosig hardware and the collected responses are processed further using DATS software.

The plate specimen is excited with 10% burst random signal. The frequency band of interest has been kept as 0-128 Hz, with a frequency resolution of 0.25 (512-time samples).The time domain signals of both force transducer and response accelerometer are monitored on line. Twenty averages of the time responses have been used to obtain the noise free response signal by maintaining adequate quality of measurement. Uniform window is applied to both excitation and response signals to have leakage free data. Programmable anti-aliasing filters are also used for both excitation and response channels to avoid aliasing errors. Transfer functions are calculated using traditional H1 method between a response signal (acceleration) and a reference signal (force) and are stored. Fig.4 shows the typical frequency response function (FRF) for the tip response. The FRF is then fed into stabilization algorithm to identify the stable modes. The frequencies and modal damping are calculated for the identified stable modes.

Modelling of the Experimental Structure

A 2D finite element model is generated in FEMAP to compute the free vibration characteristics of composite plate specimen. The four-node quadrilateral laminated plate elements are used (512 in total) to analyze the plate specimen in NASTRAN. The stacking sequence of $[0/90/0/90/0/90/0/90/0/90/0/90]_T$ is used to idealize the

twelve plies laminate configuration. The properties used in the modeling of the laminated specimen are given in Table-1. Finite element model of the plate, sensor locations and the boundary condition applied are shown in Fig.5. The finite element analysis is performed in MSC/NASTRAN to determine the frequencies and modeshapes of the plate specimen. The frequency and modeshape comparison between experiment and FEA analysis are tabulated in Table-3. A good agreement is observed between experiment and finite element analysis results.

Multifunctional Structure Calibration and Results

The frequency response analysis is performed on the finite element model of the laminated plate specimen using MSC/NASTRAN to compute the strain values around the critical frequencies. A location is selected at 75mm from the leading edge and 10mm from the fixed end to excite the finite element structural model. Strains are computed by exciting the specimen with constant input dynamic force of 1.0N around the critical frequencies. The modal damping values of the critical frequencies, which are established from the experiment have been used in the response analysis and are given in the Table-3. The computed strains at four locations (S1-S4) for the bending mode are tabulated in Table-4.

In order to measure the critical strain around the vicinity of the targeted frequencies, the laminated composite plate is excited using a shaker at a location similar to the FE analysis. The measured strains at four different locations (S1-S4) are tabulated in Table-5. From Tables-4 and 5, it can be noticed that there are discrepancies in the computed strains; therefore if these values are considered for calibrating the distributed multifunctional sensors that may introduce significant error. For an efficient sensor calibration in the multifunctional structure, the error between the computed and the actual strain/charge must be reduced. Hence, in the present study a hybrid approach is developed; in which the GVT measured damping values of the critical modes are first incorporated, while estimating the responses in the FEM analysis. The difference in the measured strain and the computed strain at reference location is then estimated in terms of percentage. The calculated error is subsequently applied on the FE computed strains at all monitoring locations to obtain the expected strains. The expected strains and the measured strains are presented in Table-6. By applying this procedure, it has been shown that the multiple sensors can be validated in the numerical model (multifunctional structure) through a limited number of measurements (see Table-6). Further, using these expected strain values (FE updated), the charge based PZT thin patches/films can be calibrated to output the engineering strains for response monitoring.

The PZT responses are also monitored for the bending mode of the plate specimen at four different locations (P1 to P4) in order to calculate the dynamic calibration factor. The dynamic calibration factors (DCF) are subsequently

Table-3 : Comparison between Experiment and FEA Results

Experiment		FEA Frequency (Hz)	Mode Description
Frequency (Hz)	Damping (%)		
42.37	1.87	42.43	Bending
80.17	1.69	80.87	Torsion

Table-4 : Computed Strains from FEA

Frequency (Hz)	Micro Strain			
	S_{ref}	S2	S3	S4
41.0	22.66	6.33	25.51	22.33
41.5	33.20	9.35	38.70	32.70
42.0	55.16	15.65	66.44	54.30
42.5	75.91	21.69	94.29	74.70
43.0	49.58	14.26	63.39	48.77
43.5	31.69	9.17	41.64	31.11
44.0	22.88	6.66	30.5	22.48

Table-5 : Measured Strains

Frequency (Hz)	Micro Strain			
	S_{ref}	S2	S3	S4
41.0	27.3	8.48	26.30	26.04
41.5	37.8	12.15	40.66	37.85
42.0	55.31	17.94	65.15	56.47
42.5	66.67	21.73	84.60	68.88
43.0	52.29	17.08	71.19	53.98
43.5	35.62	11.77	53.27	36.5
44.0	26.23	8.84	40.87	27.7

computed based on the expected strain and sensor voltage at each location. Table-7 presents the PZT sensor voltage at different locations and the corresponding DCFs. From Table-7, the average DCF's are 132,162, 84 and 125 for the locations 1, 2, 3, and 4 respectively. Experiments are repeated for different dynamic loads and PZT responses are collected at different locations. Subsequently the equivalent strains are calculated based on the DCF's (refer to Table-7) for the measured PZT responses. Table-8 displays the measured PZT responses, the calculated equivalent strains using DCF's and also the measured strains of strain gauges for different dynamic loads. There is a close agreement observed between the PZT strains and measured strains by gauges. In order to validate the developed multi-sensor calibration procedure, another location 4 (Fig.2 : SS3) has been chosen as reference sensor. Further, the expected strains for all the other sensors (strain gauges / PZT's) are then computed and subsequently DCF's are estimated. The expected strains and the measured strains are presented in Table-9. Table-10 gives the PZT sensor voltage at different locations and the corresponding DCF's. From the Table-10, the computed average DCF's are 137,167, 87 and 129 for the locations 1, 2, 3, and 4 respectively. The equivalent strains are calculated based on the DCF's for the measured PZT responses for different dynamic loads. Table 11 displays the measured PZT responses, the calculated equivalent strains using DCF's and also the measured strains of strain gauges for different dynamic loads. There is a close agreement observed between the PZT strains and measured strains by gauges. Therefore, it is noticed that the updated FEM strains using optimal measurement can be exploited

Table-6 : Comparison between Expected Strain and Measured Strain

Frequency (Hz)	Micro Strain							
	S1 (exp)	S1 (X)	S2 (exp)	S2 (X)	S3 (exp)	S3 (X)	S4 (exp)	S4 (X)
41.0	27.3	27.3	7.62	8.48	30.73	26.30	26.90	26.04
41.5	37.8	37.8	10.64	12.15	44.06	40.66	37.23	37.85
42.0	55.31	55.31	15.69	17.94	66.62	65.15	54.44	56.47
42.5	66.67	66.67	19.04	21.73	82.81	84.60	65.60	68.88
43.0	52.29	52.29	15.03	17.08	66.85	71.19	51.43	53.98
43.5	35.62	35.62	10.30	11.77	46.80	53.27	34.96	36.5
44.0	26.23	26.23	7.63	8.84	34.96	40.87	25.77	27.7

exp : expected X : experiment

Table-7 : PZT Response and Dynamic Calibration Factor (DCF) for 1 N Force

Frequency (Hz)	PZT Response (V)				DCF ($\mu\varepsilon$ / V)			
	P1	P2	P3	P4	S_{Xref} / P1	$S2_{exp}$ / P2	$S3_{exp}$ / P3	$S4_{exp}$ / P4
41.0	0.20	0.04	0.25	0.2	136.5	190.65	122.93	134.51
41.5	0.27	0.06	0.44	0.28	140.0	177.42	100.14	132.96
42.0	0.41	0.10	0.75	0.43	134.90	156.92	88.82	126.62
42.5	0.51	0.12	1.02	0.53	130.72	158.74	81.188	123.78
43.0	0.4	0.10	0.91	0.42	130.72	150.39	73.46	122.46
43.5	0.27	0.07	0.70	0.29	131.92	147.24	66.86	120.57
44.0	0.21	0.05	0.57	0.22	124.90	152.70	61.34	117.14

Table-8 : PZT Response, Calculated Strain using DCF's and Measured Strain (0.7N Force)

Frequency (Hz)	PZT Response (V)				Calculated Using DCF (με)				Measured Strain (με)			
	P1	P2	P3	P4	S1	S2	S3	S4	S1	S2	S3	S4
41.0	0.14	0.05	0.22	0.14	18.59	8.10	18.69	17.56	19.38	6.18	16.44	20.77
41.5	0.23	0.08	0.4	0.22	30.54	12.96	33.98	27.59	29.09	9.11	28.17	31.4
42.0	0.34	0.1	0.63	0.34	45.15	16.20	53.53	42.64	43.12	13.91	46.66	48.01
42.5	0.39	0.11	0.75	0.39	51.79	17.82	63.72	48.92	49.12	16.06	58.57	55.35
43.0	0.3	0.09	0.66	0.32	39.84	14.58	56.08	40.14	38.39	12.46	49.71	42.89
43.5	0.22	0.08	0.51	0.23	29.22	12.96	43.33	28.85	26.7	8.99	36.93	30.46
44.0	0.17	0.07	0.42	0.18	22.57	11.34	35.68	22.57	19.21	6.35	29.59	22.46

Table-9 : Comparison between Expected Strain and Measured Strain (Reference - Location 4)

Frequency (Hz)	Micro Strain							
	S1 (exp)	S1 (X)	S2 (exp)	S2 (X)	S3 (exp)	S3 (X)	S4 (exp)	S4 (X)
41.0	26.42	27.3	7.38	8.48	29.74	26.30	26.04	26.04
41.5	38.42	37.8	10.82	12.15	44.79	40.66	37.85	37.85
42.0	57.36	55.31	16.27	17.94	69.09	65.15	56.47	56.47
42.5	69.99	66.67	20.00	21.73	86.94	84.60	68.88	68.88
43.0	54.87	52.29	15.78	17.08	70.16	71.19	53.98	53.98
43.5	37.18	35.62	10.75	11.77	48.85	53.27	36.5	36.5
44.0	28.19	26.23	8.20	8.84	37.58	40.87	27.7	27.7

exp : expected X : experiment

Table-10: PZT Response and Dynamic Calibration Factor (DCF) for 1 N Force (Reference - Location 4)

Frequency (Hz)	PZT Response (V)				DCF (με / V)			
	P1	P2	P3	P4	$S1_{exp}$ / P1	S2exp / P2	$S3_{exp}$ / P3	S_{Xref} / P4
41.0	0.20	0.04	0.25	0.2	132.12	184.54	188.99	130.2
41.5	0.27	0.06	0.44	0.28	142.32	180.37	101.80	135.17
42.0	0.41	0.10	0.75	0.43	139.91	162.75	92.12	131.32
42.5	0.51	0.12	1.02	0.53	137.24	166.66	85.23	129.96
43.0	0.4	0.10	0.91	0.42	137.19	157.83	77.10	128.52
43.5	0.27	0.07	0.70	0.29	137.70	153.69	69.79	125.86
44.0	0.21	0.05	0.57	0.22	134.25	164.12	65.93	125.90

Table-11 : PZT Response, Calculated Strain using DCF's and Measured Strain (0.7N Force)

Frequency (Hz)	PZT Response (V)				Calculated Using DCF (με)				Measured Strain (με)			
	P1	P2	P3	P4	S1	S2	S3	S4	S1	S2	S3	S4
41.0	0.14	0.05	0.22	0.14	18.59	9.226	26.17	18.22	19.38	6.18	16.44	20.77
41.5	0.23	0.08	0.4	0.22	32.73	14.43	40.72	29.73	29.09	9.11	28.17	31.4
42.0	0.34	0.1	0.63	0.34	47.57	16.27	58.03	44.65	43.12	13.91	46.66	48.01
42.5	0.39	0.11	0.75	0.39	53.52	18.33	63.92	50.68	49.12	16.06	58.57	55.35
43.0	0.3	0.09	0.66	0.32	41.15	14.20	50.88	41.12	38.39	12.46	49.71	42.89
43.5	0.22	0.08	0.51	0.23	30.29	12.29	35.59	28.94	26.7	8.99	36.93	30.46
44.0	0.17	0.07	0.42	0.18	22.82	11.48	27.69	22.66	19.21	6.35	29.59	22.46

for the effective calibration of distributed PZT sensors to output engineering strains.

Observations

The calculated strain values from DCF's and the measured ones are compared; the following observations are made:

- Based on the reference strain gauge data the error minimization is performed on all the PZT patches.
- The PZT patch strain that is located near to the reference strain gauge, shows a reduced error compared to far away patches with respect to the measured strain gauge values, near by in their vicinity.
- The symmetrically located PZT patches display an improved accuracy, after error minimization using the reference strain gauge value. This clearly explains that symmetrically placed substructures can be grouped as one for multi-sensors calibration process, besides those placed near by.

Conclusions

Procedures are developed to calibrate the surface bonded PZT sensors in-situ on composite structure. Using a reference strain gauge output and FE strain data, it is shown that the multiple PZT patches can be calibrated. Thus the structure is made to behave multifunctionally and output its response that can be quantified for the purpose of monitoring its health. Further, through a sub-structuring process, it has been shown that the importance of reference sensor location in multi-sensors calibration approach. The developed scheme is directly applicable for any types of sensors, namely PZT thin films, FBG sensors etc in load monitoring and damage prediction solutions.

Acknowledgements

The authors gratefully thank Mr S. Shivaprasad, Scientific Assistant and Mr Chethan, Project Graduate Trainee for all the help rendered in instrumenting the specimen, data acquisition and testing.

References

1. Sathyanarayana, C.N and Raja, S., "Procedure to Monitor the Critical Dynamic Strain Through PZT Sensor", Proceedings of XVI National Seminar on Aerospace Structures (XVI NASAS), 2009.

2. Wei Fan and Pizhong Qiao., "Vibration-based Damage Identification Methods: A review and Comparative Study", Structural Health Monitoring Online First, Published on 20, 2010.

3. Jinping Ou and Hui Li, "Structural Health Monitoring in Mainland Chain: Review and Future Trends", Structural Health Monitoring Online First, Published on March 16, 2010.

4. Phillps A Adewuyi., Zhishen Wu and Kammrujaman Serker, N.H.M., "Assessment of Vibration-based Damage Identification Methods Using Displacement and Distributed Strain Measurements", Structural Health Monitoring, Vol 8(6), 2009, pp.443-461.

5. Adewuyi, A. P and Wu, Z. S., "Vibration-Based Structural Health Monitoring Technique using Statistical Features from Strain Measurements", Journal of Engineering and Applied Sciences, Vol 4, No 3, 2009, pp.38-47.

6. Kamrujjaman Serkar, N. H. M and Wu, Z. S., "Structural Health Monitoring Using Distributed Macro-Strain Response", Journal of Applied Science, 9(7), 2009, pp.1276-1284.

7. Ajay Kesavan., Sabu John and Israel Herszberg., "Strain-based Structural Health Monitoring of Complex Structures", Structural Health Monitoring, Vol.7(3), 2008, pp.203-211.

8. Takeda, N., Okabe, Y and Mizutani, T., "Damage Detection in Composite using Optical Fibre Sensors", Proceedings of the Institution of Mechanical Engineers, Part G: Journal of Aerospace Engineering, Vol. 221, No 4, 2007, pp.497-508.

9. Ashwin, U., Raja, S and Dwarakanathan, D., "A Finite Element Based Substructuring Procedure for Design Analysis of Large Smart Structural Systems", Smart Material and Structures, Vol.18, 2009.

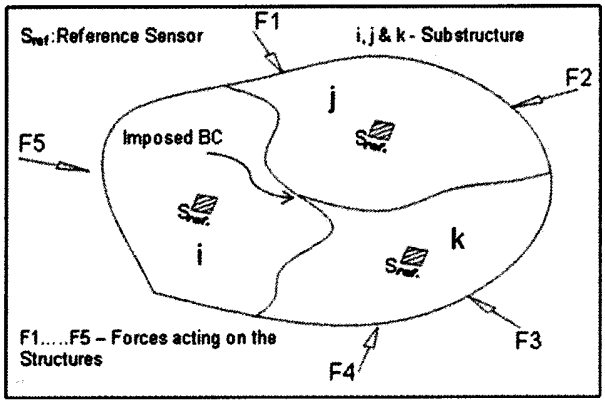

Fig.1 Sub Structuring for Effective Sensor Calibration

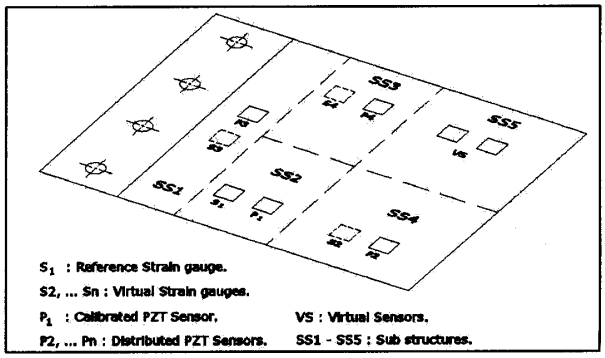

Fig.2 Virtual Strain Gauges and Distributed PZT for Multi-Sensor Calibration

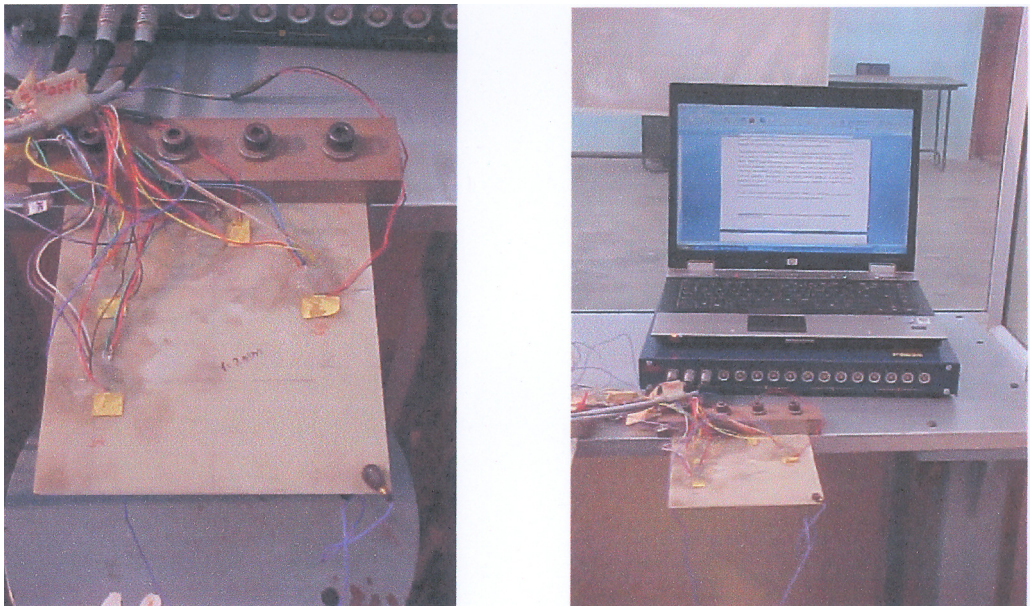

Fig.3 Experimental Test Setup for Multi-Sensor Calibration

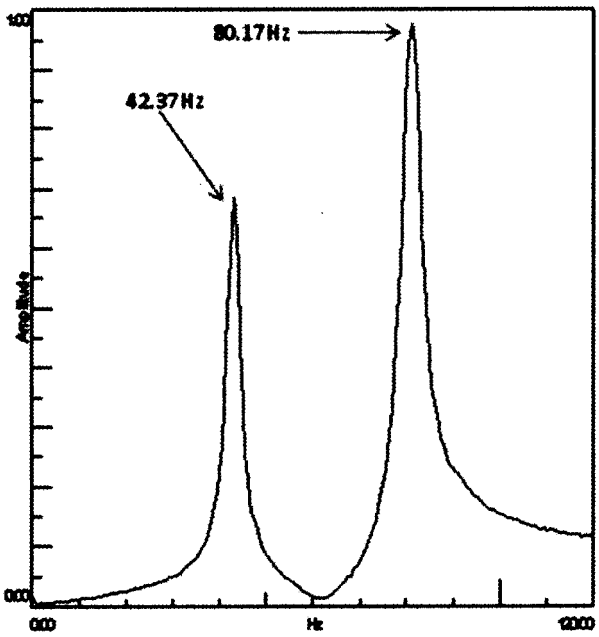

Fig.4 Frequency Response Function

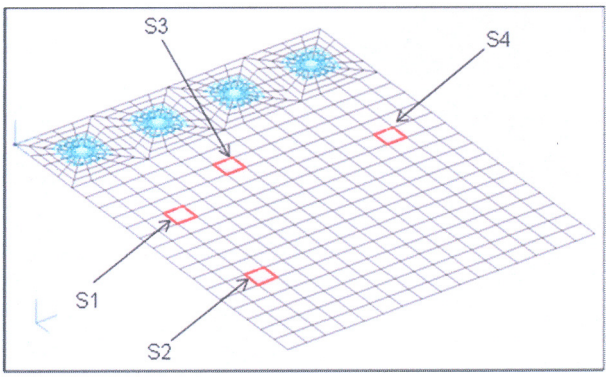

Fig.5 Strain Response Locations on FE Model